Available online at www.sciencedirect.com
SCIENCE DIRECT
Earth and Planetary Science Letters 241 (2006) 422–437
EPSL
www.elsevier.com/locate/epsl

High temperatures and inverted metamorphism in the schist of Sierra de Salinas, California

Steven Kidder *, Mihai N. Ducea

Department of Geosciences, University of Arizona 1040 E. 4th St., Tucson, AZ, 85721, United States

Received 21 June 2005; received in revised form 26 November 2005; accepted 27 November 2005
Available online 5 January 2006
Editor: R.D. van der Hilst

Abstract

New field and thermobarometric work in the Californian Salinian block clarifies current and pre-Tertiary relationships between the schist of Sierra de Salinas and Cretaceous arc-related granitic rocks. The contact is variably preserved as a brittle fault and high-temperature mylonite zone, the Salinas shear zone, which represents the contact between North America and sediments accreted above the Farallon slab between ~76 Ma and ~70 Ma. Near granulite facies, prograde replacement of hornblende with clinopyroxene is associated with deformation of plutonic rocks at the base of the upper plate. In the lower plate, the schist of Sierra de Salinas, garnet–biotite thermometry indicates decreasing temperatures down-section from at least 714 °C to ~575 °C over an exposed thickness of ~2.5 km, consistent with petrologic evidence of an inverted metamorphic gradient. The measured temperatures are significantly higher than observed at shallow levels above subducting slabs or predicted by 2D computational models assuming low shear stresses. Previous workers have called upon shear heating to explain similar observations in the correlative Pelona schist, an unlikely scenario given the results of recent rock deformation experiments which predict that feldspar–quartz–mica aggregates are far too weak to withstand stresses of ~70 MPa required by the shear heating hypothesis. As an alternative, we propose that high temperatures resulted from conductive heating while the leading edge of the schist traveled ~150 km beneath the recently active Salinian continental arc during the initiation of shallow subduction. Weakening of the schist due to high temperatures helped facilitate the collapse of the Salinian arc as the schist was emplaced. Schist emplacement coincided with loss of lower, mafic portions of the arc, and therefore evolution of the Southern California crust towards a more felsic composition.

Keywords: shear heating; subduction; POR schists; Salinia; schist of Sierra de Salinas; Pelona schist; accretion

1. Introduction

Temperature and stress in the lithosphere are closely linked. Psuedotachylytes provide striking evidence that under certain conditions, high stresses induce deformation that sharply raises temperatures on a scale of meters. The heat generated is related to stress by the relationship $Q_{sh}=c\tau V$, where Q_{sh}=rate of shear heating, τ=shear stress, V=slip rate, and c is the percentage of mechanical work converted to heat. In a ductile regime, $c=90\pm5$ [1], and stress and temperature are linked through flow laws (e.g. [2,3]) such that with increasing temperature, the stress required to achieve a given strain rate decreases exponentially and shear heating becomes increasingly less significant.

While these general relationships are straightforward, significant uncertainties remain regarding the

* Corresponding author. Present address: California Institute of Technology, Division of Geological and Planetary Sciences, MC 170-25, 1200 E. California Blvd., Pasadena, CA 91125, United States.
E-mail address: kidder@gps.caltech.edu (S. Kidder).

0012-821X/$ - see front matter © 2005 Elsevier B.V. All rights reserved.
doi:10.1016/j.epsl.2005.11.037

magnitude of lithospheric stresses and the thermal effects of deformation in tectonically active regions [4–6]. Viscous or "fluid" deformation of crystalline lower crust at temperatures above 600–700 °C involves low stresses: between 10^{-2} and 10^{-5} MPa given calculated viscosities of 10^{16}–10^{19} Pa s (e.g. [7–11]) and a "geologic" strain rate of 10^{-15} s^{-1} (e.g. [8,12]). In contrast, much higher stresses (30–430 MPa) are required if extensive shear heating is responsible for km-scale thermal anomalies in which quartzofeldspathic rocks reach temperatures of 650–750 °C (referred to here as the "shear heating hypothesis") [13–18]. Thermal and thermal-mechanical models are particularly subject to ambiguities regarding shear heating, to the extent that one goal of many modeling efforts is estimating the extent to which shear heating affects thermal conditions in the lithosphere (e.g. [4,5,16,17,19–24]).

The Pelona schist (Fig. 1), considered by most workers an early Tertiary subduction complex (e.g. [25]), has served as a type example in arguments that shear heating can play an important role in crustal metamorphism along major shear zones [13–16]. Based on temperatures as high as 650 °C in an inverted metamorphic gradient in the Pelona schist, shear stresses are estimated to have been 130 MPa [13], 40 MPa [15] and 70 MPa [16]. Temperatures achieved in the Pelona schist at depths of ~40 km are significantly higher than predicted by thermal models of subduction zones incorporating low shear stresses (e.g. [5,20,26,27]); however, as described below, quartzofeldspathic rocks are not generally expected to retain enough strength to support such high stresses at the observed temperatures. No alternative explanations for high temperatures in the Pelona schist have been proposed.

We carried out field and thermobarometric work in the schist of Sierra de Salinas (Fig. 1), a correlative of the Pelona schist, and document peak temperatures of at least 714 °C in an inverted metamorphic gradient. This temperature is ~300 °C higher than the average of well constrained upper and lower plate temperatures prior to structural juxtaposition. The Late Cretaceous shear zone is partially exposed, and we document an upper amphibolite facies, prograde metamorphic reaction associated with deformation. These observations raise the question of whether shear heating played an important role in metamorphism of the schist. We address this question by considering the broader tectonic setting under which deformation occurred, and by comparing compositional and microstructural characteristics of the schist with the predictions of various rock deformation experiments on quartzofeldspathic rocks. Our analysis indicates that the schist was too weak to support stresses required by the shear heating hypothesis. We propose that conductive heating associated with the initiation of shallow subduction provides a better explanation for heating of the schist of Sierra de Salinas and correlative Pelona schist.

2. Geologic background

The fault bounded Salinian block (Fig. 1) exposes middle crustal levels of a Cretaceous continental arc and an underplated Cretaceous metagraywacke known as the schist of Sierra de Salinas (referred to here as "the schist;" [28,29]). The Salinian block was displaced from its Cretaceous location west of the Mojave region (e.g. Fig. 1; [30,31]) and transported to its present location in central California by ~330 km of right-lateral slip along the San Andreas fault [32].

The schist of Sierra de Salinas crops out in two structural windows and a few isolated exposures in the Salinian block (Fig. 1; [28]). Correlatives of the schist of Sierra de Salinas include the Pelona, Orocopia and Rand schists (referred to here as the "POR schists;" Fig. 1). Structural relationships indicate that the POR schists represent a regional lower plate in a large area of southern California and southwest Arizona, and most workers believe that the POR schists represent underplated accretionary wedge correlatives of the Franciscan assemblage or possibly Great Valley sequence, which were progressively deposited, subducted, and carried eastward beneath the Southern California continental arc from 90–50 Ma during flat slab subduction (e.g. [33,34]). While deposition of the protoliths of the POR schists occurred throughout a 40 Myr period, individual exposures were deposited, subducted to depths of 30–40 km, and exhumed in quick succession, in at least some cases under 3 million years [33]. In Salinia, these events occurred during a time period marked in the upper plate by the cessation of arc-related magmatism at ~81 Ma and the appearance of 7–8 kbar arc-related rocks at the surface at 68–69 Ma [35].

Salinian plutonic rocks are similar in age, composition, and isotopic characteristics to plutonic rocks found on the eastern side of the Sierra Nevada and Peninsular Ranges batholiths ([29,36,37]; Fig. 1). Where autochthonous, the eastern batholithic rocks of the California arc are found ~150 km east of the associated Franciscan accretionary assemblage (Fig. 1). The juxtaposition of the Salinian plutonic rocks against the schist, as well as Salinia's pre-San Andreas location 100–150 km west of similar eastern-affinity batholithic rocks in the central Sierra Nevada and Peninsular Ranges (Fig. 1), suggests 100–150 km of offset between the Salinian arc and the

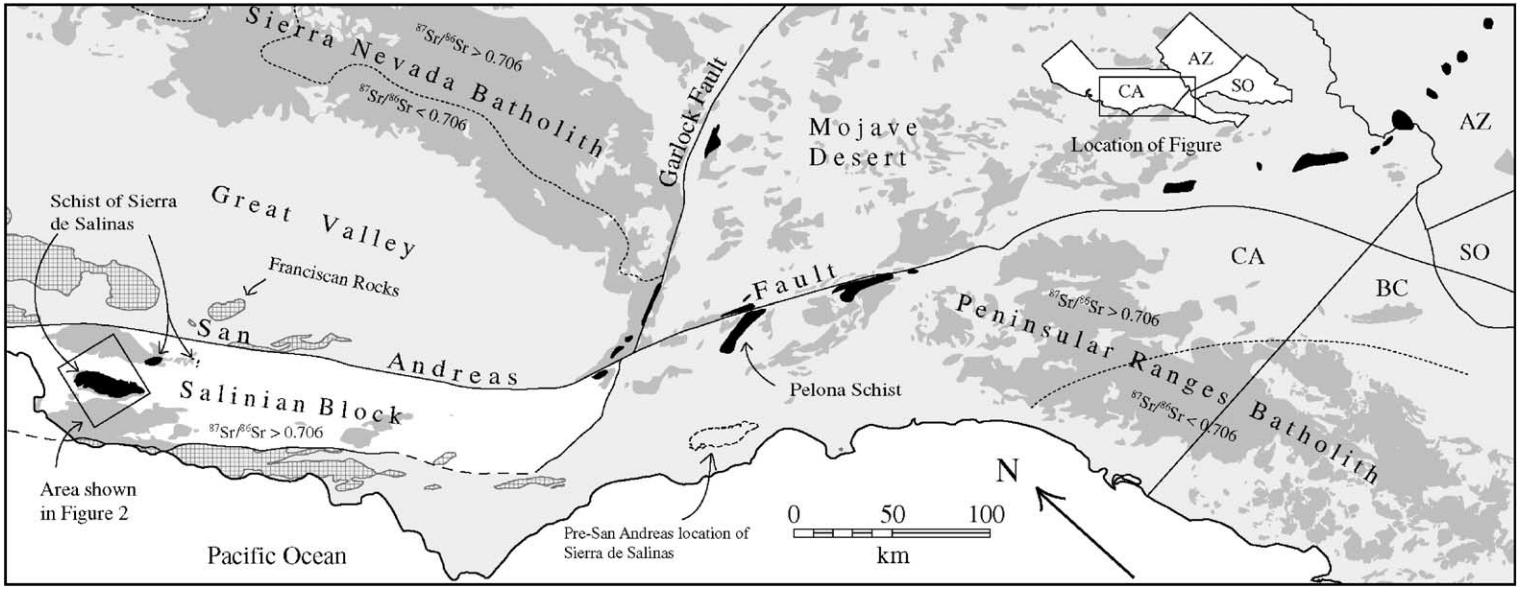

Fig. 1. Map of parts of California, Arizona, Sonora, and Baja California showing geologic features discussed in the text. The POR schists are shown in black. Mesozoic granitic and related metamorphic rocks are shaded lightly. Dotted lines separate zones of western and eastern batholithic rocks as indicated by $^{87}Sr/^{86}Sr$ isopleths. Fine-gridded areas are mainly Franciscan formation. The restored location of the Sierra de Salinas is based on palinspastic reconstruction prior to disruption by the San Andreas Fault system at ~20 Ma [32]. Restoration is relative to the southern Sierra Nevada.

schist of Sierra de Salinas [30,38]. Based on $^{40}Ar/^{39}Ar$ cooling ages and U–Pb analyses of detrital zircons in the schist of Sierra de Salinas, Barth et al. [39] proposed that this juxtaposition occurred in the Late Cretaceous, a conclusion supported by the work presented in this paper. The "missing" western side of the Salinian arc, fragments of which remain in Gualala basin conglomerates [40], was carried even farther west and either buried, eroded, subducted, or carried to the north along Tertiary strike slip faults (e.g. [34,37,40]).

3. Methods

Electron microprobe analyses were conducted at the University of Arizona using a Cameca SX50 microprobe equipped with 5 LiF, PET and TAP spectrometers. Counting times for each element were 30 s at an accelerating potential of 15 kV. A beam current of 20 nA and width of ~1.8 μm were used for garnet analyses. To lessen alkali volatility, a beam current of 20 nA and width of 5 μm were used on plagioclase, biotite, and hornblende, except for K and Na, which were analyzed at a beam current of 10 nA. Unless otherwise noted, garnets and plagioclase with totals outside of the range 100% ± 1, biotites with totals outside of the range 94% ± 1, and hornblendes with totals outside the range 97–98.3% were discarded. Plagioclase with poor stoichiometry and hornblende analyses which failed the compositional criteria of Papike [41] were discarded. A few biotites in each sample were analyzed for chromium and nickel. Measured totals fell near or below detection levels, and these elements were not measured in subsequent analyses.

We used a formulation of the garnet–biotite thermometer by Ganguly and Cheng (unpublished computer program), which utilizes the experimental data of Ferry and Spear [42] in the Fe–Mg binary system, and the mutually compatible biotite and garnet solution models of Ganguly et al. [43]. Fe^{3+} contents were estimated as 3 mol% of total Fe in garnet and 11.6 mol% of total Fe in biotite based on the average values for metapelites used by Holdaway [44]. Estimates assuming Fe^{2+}=Fe(total) yield temperatures 23–32 °C higher than those calculated using the empirical Fe^{3+} correction. Representative biotites were found to have low but measurable F and Cl concentrations. F and Cl temperature corrections for the garnet–biotite thermometer follow Zhu and Sverjensky [45].

We used the garnet–hornblende thermometer of Graham and Powell [46] and two formulations of the Garnet–Biotite–Plagioclase barometer of Hoisch [47]. To calculate pressures, we used the average value of Hoisch's equilibria where it is intersected by the garnet–biotite exchange equilibrium.

4. Results

4.1. Structure and petrology of the schist

The main exposure of the schist underlies the Sierra de Salinas, a northwest trending range southwest of the Salinas valley (Fig. 2). The schist is bounded on the northeast by the Rinconada fault, on which ~44 km dextral slip occurred in the late-Tertiary [37]. Barth et al. [39] found that the Cretaceous granitic rocks to the southwest and northwest of the schist are older than the schist and could not have intruded it as proposed by Ross [28]. Our field observations indicate that along much of the southwest flank of the range, the contact between the schist and granite is marked by a steep, southwest-dipping brittle fault. In other areas, a partially exposed ductile shear zone, which we name the Salinas shear zone, separates the schist and granite. Along the southwest side of the range, both upper and lower plate rocks near the brittle fault display features similar to rocks in the ductile shear zone, indicating a component of normal faulting which cuts out no more than 1 or 2 km of section.

The schist has a southwest-dipping monoclinal form in most of the range, but dips to the northwest in northwestern exposures (Fig. 2). Both the schist and adjacent granites are overlain by Miocene sedimentary rocks which dip gently to the southwest and northwest away from schist. These orientations mimic those in the schist, indicating that prior to post-Miocene tilting, foliation in the schist approached horizontal. Structurally "higher" and "lower" levels of the schist are thus approximated by structural distance from the schist–granite contact along the southwest and northwest sides of the range.

The schist is homogeneous in appearance, with the exception of quartz veins, and dikes and veins composed predominantly of quartz, plagioclase and potassium feldspar. Observed quartzofeldspathic veins range from a few mm to 20 cm in thickness. Although they occasionally cut foliation at high angles, the quartzofeldspathic veins are generally concordant and often asymmetrically folded with the schist (Fig. 3). Quartzofeldspathic veins are most common at higher structural levels, but are found throughout the schist and presumably indicate syndeformational partial melting of the schist near the wet solidus. Veins and blobs composed predominantly of quartz are widespread,

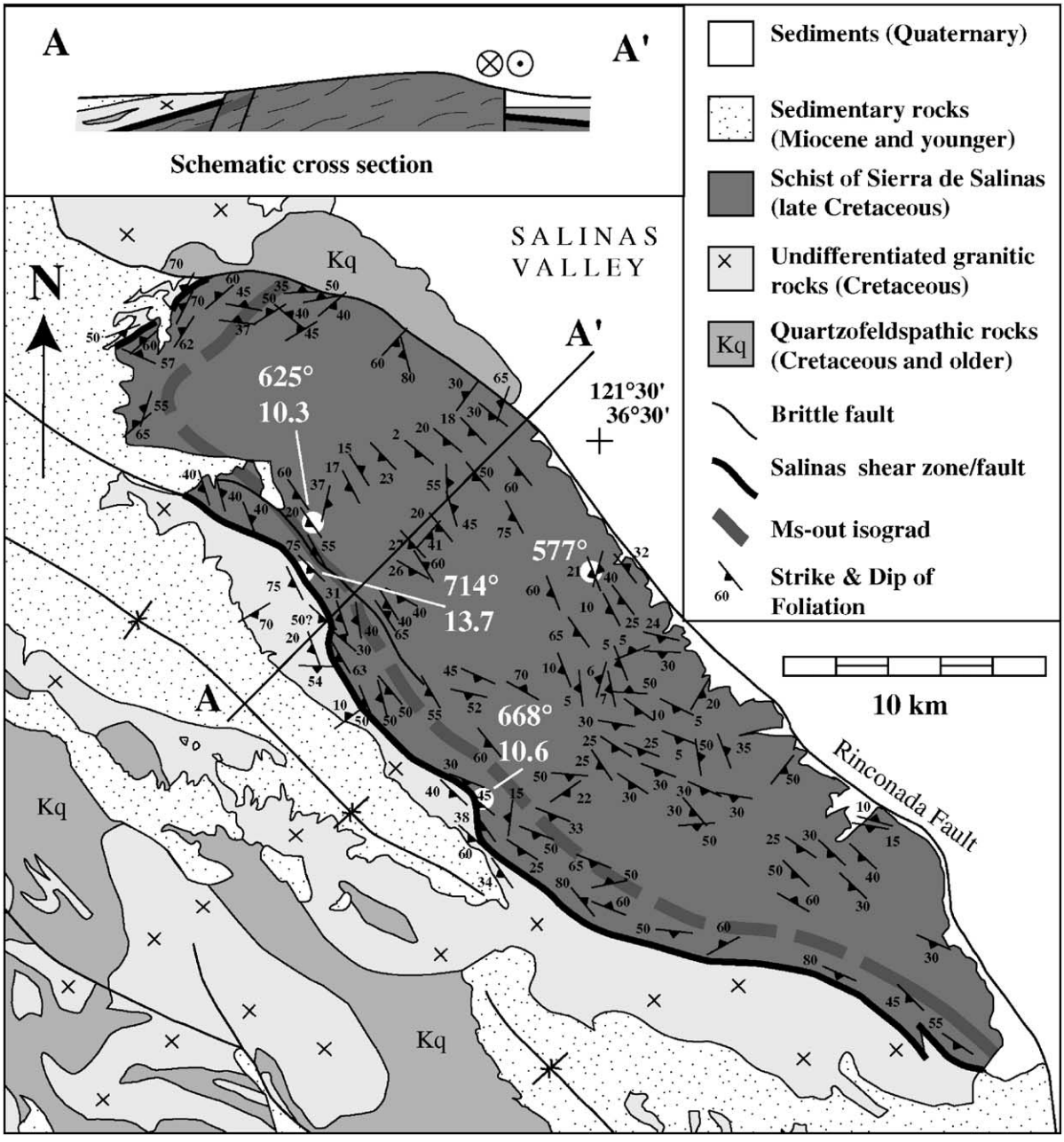

Fig. 2. Geologic map of the Sierra de Salinas and surrounding area. Structural data from Ross [28], Dibblee [76] and this study. White circles show locations of thermobarometric measurements (temperature (°C), pressure (kbar)). No primary muscovite was found west of the ms-out isograd. See Table 2 for sample names.

but less common than the quartzofeldspathic veins. In thin section, quartz grains—in veins and in thin, foliation-parallel quartz band—display evidence of extensive dynamic recrystallization, including undulose extinction, development of subgrains and lattice preferred orientation. Quartz grains display a "chessboard subgrain pattern" (e.g. [48]) indicating the preservation of high temperature microstructures.

Based on observation of 20 thin sections and the work of Ross [28], the schist contains 40–50% plagioclase ($An_{15–40}$), which range in diameter from 0.1–1 mm (grains ~0.5 mm in diameter dominate volumetrically). The remainder of the schist is composed of quartz (25–40%), biotite (15–20%), and in order of decreasing abundance: potassium feldspar, chlorite, muscovite, apatite, sphene, garnet, epidote, and calcic

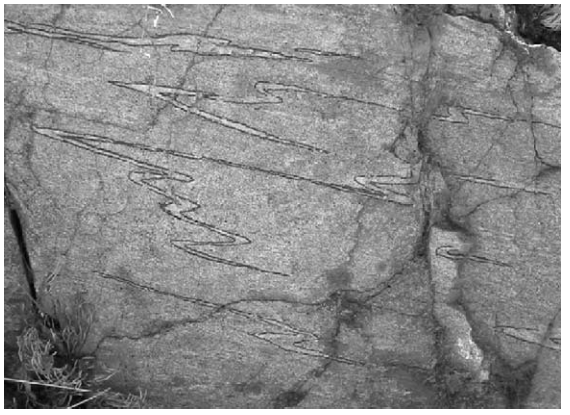

Fig. 3. Asymmetrically folded quartzofeldspathic veins (outlined in black) in the schist. Similar veins are seen throughout the schist, but are most common at highest structural levels. Field of view 50 cm.

amphibole. No aluminosilicates were identified. Mineral assemblages in the schist correlate with structural depth, such that the northwest and southwest edges of the schist are marked by an absence of primary muscovite (see ms-out isograd, Fig. 2), increased abundance of biotite, and the appearance of magnesiohornblende, actinolite and myrmekite. Plagioclase undergoes a significant change across the range related to graphite content. In thin section, plagioclase appearance ranges from dusty (graphitic) at lower structural levels, to clear (nearly graphite-free) near the contact with granitic rocks at high structural levels. Together, these observations indicate higher metamorphic grade at structurally higher levels, an observation supported by our thermobarometric work.

4.2. The schist–granite contact

The Salinas shear zone is marked by the development of mylonitic foliation in upper plate hornblende–quartz diorite (Fig. 4a–c). Over a distance of ~100 m, the coarse-grained hornblende–quartz diorite grades

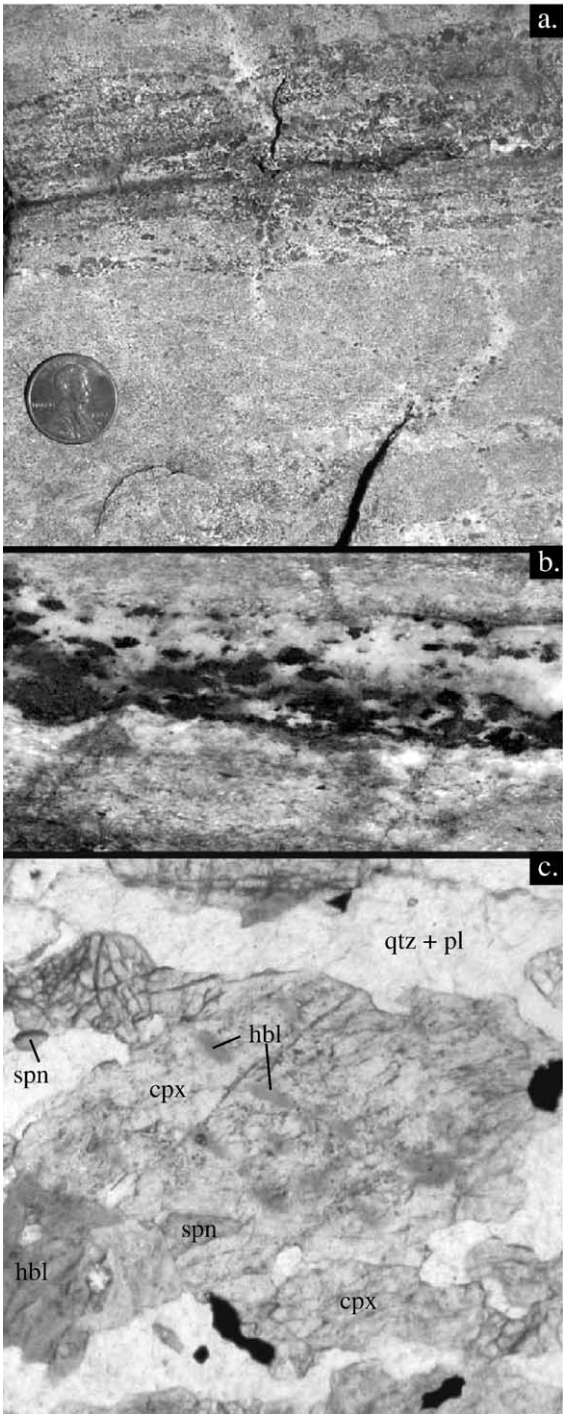

Fig. 4. Photographs of deformed hornblende quartz diorite (upper plate) in the Salinas shear zone. (a) Hornblende-rich band (darker layers in upper half of photo) preserved in the clinopyroxene-dominated mylonite. Hornblende-rich areas: pl+brown hbl+qtz+spn; Clinopyroxene-rich areas: qtz+pl+cpx+spn ± czo ± green hbl. White-colored veins composed predominantly of pl+qtz+hbl cut foliation planes in the center and right side of the photo. Field of view, 12.5 cm. (b) Close up of inter-layered hornblende and clinopyroxene-rich foliation in a different sample. Dark hornblendes are preserved in coarser, less deformed layers. Hornblende was reduced in size and recrystallized to form clinopyroxene in highly deformed layers as part of a prograde, transitional amphibolite–granulite facies reaction. Layer compositions are similar to those in panel (a) Field of view, 4 cm. (c) Microphotograph showing a commonly observed relationship in which hornblende inclusions of shared orientation occur within a larger clinopyroxene grain. Matrix hornblendes such as the one seen in the lower left may be remnants of original hornblende grains or may be associated with hornblende-bearing veins which cut foliation. Plane polarized light. Field of view, 1 mm.

towards the schist into a foliated, finer-grained mylonite. Clinopyroxene becomes the major, and sometimes only, mafic phase with increasing degree of mylonitization. The absence of clinopyroxene elsewhere in upper plate rocks within a few km of the shear zone, and patchy remains of formerly continuous hornblende grains in clinopyroxene (Fig. 4c) indicate growth of clinopyroxene at the expense of hornblende. The association of deformation with the appearance of clinopyroxene is further highlighted by small scale layering in which hornblende and clinopyroxene alternate as the predominant mafic phase (Fig. 4a, b). Clinopyroxene bands have finer grain size and a higher concentration of quartz, while coarse-grained hornblende is preserved in more plagioclase-rich layers. Both smaller grain size and higher quartz content contribute to weakening the clinopyroxene-bearing layers, which appear microstructurally to have experienced more ductile shearing. Given their small thicknesses, the layers experienced the same pressure-temperature conditions, thus we suggest that hornblende survived metastably in the less deformed layers while deformation activated the clinopyroxene forming reaction in more quartz-rich layers. Small scale variations in fluid composition may also have played a role in stabilizing hornblende, as evidenced by mm–cm scale hornblende-bearing quartzofeldspathic veins which cut across the foliation (Fig. 4a). These veins probably represent the frozen plumbing system through which H_2O-rich fluids or melt escaped during deformation. While future work is needed to better understand these relationships, it is unambiguous that upper plate deformation was closely associated with pressure–temperature conditions near the upper stability limit of hornblende. The breakdown of hornblende to form clinopyroxene marks a transitional state between the amphibolite and granulite facies, occurring in one experiment at temperatures of 770–790 °C, 10–30° cooler than the granulite facies assemblage clinopyroxene+orthopyroxene [49].

Although lack of outcrop prevents direct observation of the schist within about 50 m of the mylonitized plutonic rocks described here, foliations and lineations in the upper and lower plates are similar across the contact.

4.3. Temperature and pressure constraints

Three garnet-bearing samples of the schist, as well as a garnet-bearing dike which cross-cuts foliation in the schist, contain assemblages considered appropriate for thermobarometric work. Forty element maps and 580 point analyses were made in order to determine inter- and intra-granular compositional variations. Mineral compositions used in thermobarometric work are reported in Table 1. Garnets in the schist display typical growth zoning (Fig. 5; [50]), with Mn and Fe# (Fe/Fe+Mg) decreasing and Ca, Fe, and Mg generally increasing from core to rim (see core and rim compositions in Table 1). We take garnet rim compositions where Fe# is lowest to represent garnet grown under peak temperature conditions. Biotite compositions vary slightly within the slides, thus biotites near garnet were considered most likely to have achieved equilibrium with garnet. A lack of Mn "kick-ups" in the garnets (e.g. [51]) and retrograde Mg–Fe phases in these slides are taken as evidence that biotites have maintained peak temperature compositions. We report thermobarometric results in Table 2.

Garnets from a dike which cross-cuts foliation in the schist (sample pgx46) are larger and more homogenized than garnets found in the schist. The muted zoning is qualitatively similar to that in the other garnets, with the exception that Fe# increases gradually toward the rim. We take the composition just inside a slight Mn kick-up in the outer 15 μm of the garnet to most closely approximate peak conditions. Seven measured biotites, both touching and not touching garnet, show no appreciable variation, and we use an average of these values in thermobarometric calculations.

As noted above, Spear [49] observed the breakdown of hornblende to form clinopyroxene in amphibolites at temperatures of 770–790 °C. These temperatures represent an alternative peak temperature estimate in the shear zone, although compositional and pressure differences (his experiments were carried out at 1 kbar) will shift these temperatures. The jadeite component in these clinopyroxenes is too small to constrain pressures.

We analyzed plagioclase compositions in 106 spots in the four samples. Compositions in most samples are fairly consistent from spot to spot. Rim compositions used in barometric estimates and standard deviations are shown in Table 1. A pressure (10 kbar) was calculated using the average composition for sample pgx16, but is not reported in Table 2 due to considerable compositional variation. Sample pgx16 also yielded the lowest garnet–biotite temperature, suggesting that the grain to grain compositional similarities in the other samples are the product of thermally induced homogenization and equilibration.

Garnet was found in mylonitized quartz diorite (sample qvf1) in the upper plate of the Salinas shear zone. Garnets as large as 1.5 cm in diameter have homogenized compositions with Mn kick-ups in the outer ~100 μm. The Mn kick-up is related to a retrograde net-transfer reaction, evident petrographically as

Table 1
Representative mineral compositions used in thermobarometric calculations

Sample	pgx7	pgx9	pgx16	pgx46	qvf1
Garnet rim					
SiO_2	37.82	38.11	37.66	37.09	*37.23*
TiO_2	0.17	0.07	0.11	0.04	*0.17*
Al_2O_3	20.86	21.72	21.17	20.68	*21.10*
Cr_2O_3	0.04	0.00	0.03	0.00	*0.03*
FeO	18.62	20.02	25.58	21.26	*28.68*
MnO	10.89	3.94	3.83	13.82	*5.00*
MgO	1.29	1.68	1.63	1.35	*2.36*
CaO	9.64	14.14	9.11	4.92	*5.56*
Total	99.4	99.7	99.2	99.2	*100.1*
Fe/(Fe+Mg)	0.89	0.87	0.90	0.90	*0.87*
n=	1	1	4	2	*1*
Garnet core					
SiO_2	*37.59*	*37.59*	*37.99*	*37.37*	38.41
TiO_2	*0.14*	*0.20*	*0.22*	*0.26*	0.23
Al_2O_3	*20.89*	*20.71*	*20.96*	*20.69*	21.55
Cr_2O_3	*0.00*	*0.05*	*0.02*	*0.00*	0.01
FeO	*12.03*	*16.28*	*15.53*	*19.47*	27.85
MnO	*20.01*	*14.42*	*14.54*	*16.51*	1.36
MgO	*0.40*	*0.60*	*0.68*	*1.42*	5.75
CaO	*8.91*	*10.22*	*10.04*	*4.03*	5.58
Total	*100.0*	*100.1*	*100.0*	*99.8*	100.8
Fe/(Fe+Mg)	*0.94*	*0.94*	*0.93*	*0.88*	0.73
n=	*1*	*1*	*1*	*1*	14
Biotite					*Hornblende*
SiO_2	36.19	36.44	36.22	35.34	43.42
TiO_2	2.34	2.58	2.99	3.23	1.75
Al_2O_3	17.36	16.55	18.03	15.71	12.14
FeO	18.07	19.08	17.25	20.66	16.90
MnO	0.36	0.42	0.36	0.66	0.27
MgO	10.01	9.34	9.67	8.42	9.67
CaO	0.03	0.03	0.01	0.00	11.38
Na_2O	0.11	0.10	0.16	0.08	1.31
K_2O	9.27	9.29	9.29	9.50	0.74
F	0.17	0.03	0.06	0.34	0.13
Cl	0.01	0.00	0.00	0.01	NA
Total	93.8	93.8	94.0	93.7	97.6
Fe/(Fe+Mg)	0.50	0.53	0.50	0.58	0.50
n=	4	5	8	7	3
Plagioclase rims					
SiO_2	60.15	58.84	61.71	61.13	*NA*
S.D.	0.40	0.90	1.68	0.27	*NA*
Al_2O_3	25.13	25.85	23.61	23.00	*NA*
S.D.	0.24	0.62	1.16	0.21	*NA*
FeO	0.06	0.09	0.12	0.05	*NA*
S.D.	0.06	0.07	0.08	0.03	*NA*
CaO	6.57	7.32	5.30	4.81	*NA*
S.D.	0.27	0.75	1.36	0.21	*NA*
Na_2O	7.86	7.46	8.74	8.86	*NA*
S.D.	0.22	0.51	0.83	0.20	*NA*
K_2O	0.21	0.18	0.16	0.21	*NA*
S.D.	0.06	0.05	0.07	0.07	*NA*

Table 1 (*continued*)

Sample	pgx7	pgx9	pgx16	pgx46	qvf1
Plagioclase rims					
Total	100.0	99.8	100.0	98.4	*NA*
n=	8	6	16	3[a]	*NA*

Garnet values in italics were not used but illustrate core and rim variation in the samples.
[a] Plagioclase totals as low as 98.3 were used in sample pgx46.

a symplectic plagioclase and biotite rim on garnets. An element map of the matrix shows a high concentration of Fe in micro-veins and cracks which we credit to the release of Fe as the garnet reacted to form plagioclase and biotite. Hornblendes, which form the major mafic matrix phase, have slightly higher Fe and Fe# cores than rims, suggesting that released Fe was not significantly absorbed by hornblende. We interpret, therefore, that the core compositions of garnet and hornblende reflect peak conditions, and use these data in calculating a temperature of 712 °C. Using the diffusion data of Cygan and Lasaga [52], the calculated temperature, and maximum time period over which deformation may have occurred (6 Myr), we calculate a characteristic length scale of diffusion [50] about an order of magnitude smaller than the radius of the garnet. This calculation suggests that insufficient temperature and time were available for the garnet core to be significantly affected by a temperature change during deformation. We conclude that the calculated temperature represents conditions prior to deformation.

4.4. Inverted thermal gradient

Based on an average dip of foliation of 21°, the inverted metamorphic gradient in the schist occurs over an exposed structural thickness of 2.5 km at an average value of ~50 °C/km. The gradient increases near the contact to a minimum value of 70 °C/km since a minor normal fault increases the apparent distance between the two highest samples (pgx7 and pgx9), and sample pgx9 was taken 200–1600 m structurally below

Table 2
Results of thermobarometric calculations

Sample	K_D[a]	T (°C)[b]	P (kbar) at calculated T
pgx7	0.125	625	10.3
pgx9	0.172	714	13.7
pgx16	0.114	577	NA
pgx46	0.156	668	10.6
qvf1	0.361	712	NA

[a] K_D is defined as the ratio $(Fe/Mg)_{bt\ or\ hbl}/(Fe/Mg)^{gt}$.
[b] Temperatures calculated at 10 kbar.

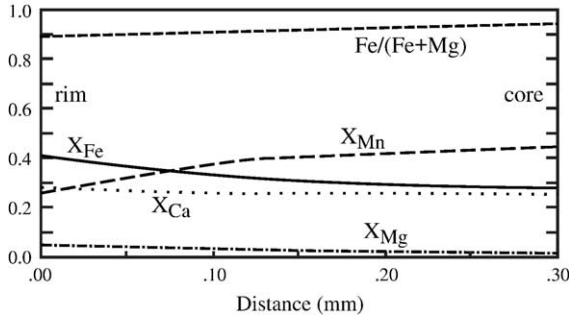

Fig. 5. Line traverse from rim to core across a small garnet in sample pgx7 showing the variation of elements.

the highest schist exposures. If similar to the Pelona schist, the temperature gradient in the upper 600–700 m of the schist may be as high as ~240 °C/km [46] and the temperature of 714 °C in sample pgx9 somewhat underestimates temperatures achieved in the shear zone. Inverted thermal gradients in the POR schists are comparable to other Cordilleran inverted gradients ranging from 30 to 330 °C/km (see e.g. [16,19]). These gradients are significantly higher than gradients of 0–13 °C/km produced in 2D models taking into account radiogenic heating, accretion and erosion (e.g. [23]), and much smaller than gradients of 4000 °C/km reported in the upper meters of ophiolite soles [53].

5. Discussion

5.1. Age of the Salinas shear zone

Lower and upper plate isotopic cooling ages are useful for dating and interpreting structural contacts between the POR schists and upper plate rocks (e.g. [25,33,39,54,55]). In the San Gabriel mountains, where the contact between schist and upper plate may represent the original subduction configuration (e.g. [54]), numerous muscovite, biotite and hornblende $^{40}Ar/^{39}Ar$ and K–Ar cooling ages in the schist and near the contact in the upper plate fall within an 8 Myr time period from 63 to 55 Ma [54]. In contrast, schist localities where structural evidence suggests multiple deformational episodes display a greater difference between upper and lower plate cooling ages. Jacobson [54] contrasted the San Gabriel mountains with the Orocopia mountains, where $^{40}Ar/^{39}Ar$ biotite ages in the schist are 25–60 Myr younger than 75–56 Ma biotite cooling ages in the upper plate [25]. In the Sierra de Salinas, Barth et al. [39] report $^{40}Ar/^{39}Ar$ biotite cooling ages of 76–75 Ma on three upper plate granitoids, as well as cooling ages of 72–68 Ma on muscovite and biotite from a southeast portion of the schist. Although there is a difference between upper and lower plate values, the cooling ages all lie within an 8 Myr window as in the San Gabriel Mountains. While more cooling data are needed nearer the Salinas shear zone, the similar upper and lower plate ages suggest a Late Cretaceous age for the Salinas shear zone. We take an age of 70 ± 1 Ma, the $^{40}Ar/^{39}Ar$ age of two biotite samples in the schist [39], to represent the latest likely age of ductile deformation and metamorphism. This interpretation is supported by our observations of near-granulite facies metamorphism associated with deformation in the shear zone, and a garnet–biotite temperature of 668 °C in a quartzofeldspathic dike cross-cutting foliation in the schist. These features developed during—or at late stages of—deformation at temperatures much higher than ~350 °C, the $^{40}Ar/^{39}Ar$ closure temperature in biotite [56]. Shearing probably did not begin before 77 ± 2 Ma, the youngest known detrital zircon age in the schist [33].

5.2. High temperatures and inverted metamorphism in the POR Schists

Graham and England [13] and England and Molnar [16] considered both the high temperatures and inverted metamorphism in the Pelona schist indicative of shear heating and high stresses. However, other workers have shown that deformation during and after metamorphism can produce inverted metamorphic gradients that are not representative of geothermal gradients that ever existed (e.g. [15,53,57]). It is clear from these studies that inverted metamorphic gradients do not generally represent inverted paleo-geotherms, and should only be considered after careful consideration of structural, barometric and chronologic data. We focus on high temperatures observed in the schists—a feature which, given narrow timing constraints for metamorphism, we consider the least ambiguous and therefore most diagnostic of the conditions traditionally explained by shear heating.

As discussed below, low temperature/pressure conditions characterize modern forearcs and forearcs recognized in the geologic record. The expectation of temperatures much lower than those measured in the POR schists is also based on the thermodynamic principle that when heat diffuses from stationary hot to cold bodies of similar size and physical properties, temperatures in the cooler body do not reach more than ~50% of the sum of the initial temperatures of the two bodies. The schist was at surface temperatures when deposited less than 7 Myr prior to cooling [33], thus in a simple model given upper plate temperatures of 700–800 °C

([35]; this paper), the schist is expected to reached a temperature no higher than 400 °C. When motion is taken into account in conduction-only 2D models of subducting slabs dipping at 45°, lower plate temperatures do not reach more than 60% of the initial temperature of the hanging wall [19]. In the remainder of the paper, we discuss the possible origin and significance of temperatures above 714 °C in the schist.

5.3. Shear heating and strength of the schist

Since the seminal work of Graham and England [13], shear heating has been the standard explanation for "excess" heat in the POR schists. England and Molnar [16] presented an equation for estimating stress in a shear zone above an inverted gradient based on lower plate temperature and other variables. If their assumptions are applicable to the POR schists, we estimate a stress of 50–90 MPa in the schist using their equation 29 with subduction angle between 5 and 20° and a Late Cretaceous convergence rate of 10 cm/yr [58]. As with the temperature of the schist, these stresses are significantly higher than stresses of order 10 MPa generally estimated in forearcs [5].

Direct evidence of shear heating may be present in the upper plate of the Salinas shear zone, where clinopyroxene replaces hornblende in the highest strained rocks (Fig. 4). Temperatures of ~780 °C [49] required for the breakdown of hornblende may have resulted from shear heating (e.g. [18]). Alternatively, sufficiently high temperatures may have existed prior to deformation (e.g. [59]) given possible errors in our upper plate temperature estimate of 712 °C. The age this temperature was achieved is currently unknown; however, Kidder et al. [35] demonstrated that one portion of the Salinian arc, the Coast Ridge Belt, was at temperatures of 700–800 °C until at least 76.5 ± 1.5 Ma.

If shear heating occurred in the upper plate, it most likely occurred prior to the replacement of the formerly-plutonic lower plate by the schist. At this early stage, high stresses would be needed to initiate shearing in undeformed, coarse-grained plutonic rocks. Strain is likely to have partitioned into the weaker schist at later stages after its arrival beneath the upper plate. Since shear heating in the upper plate, if it occurred at all, was fairly minimal and most likely occurred before arrival of the schist, we do not consider it an important heat source for the schist.

The degree to which shear heating within the schist is likely to have raised temperatures can be assessed by considering the strength of the mineral constituents of the schist, since the strengths of polyphase aggregates are generally intermediate between those of end-member phases (e.g. [60]). Extrapolations from rock deformation experiments on wet feldspar aggregates predict ductile flow at stresses of ~3 MPa given 700 °C temperatures and a strain rate of $\sim 10^{-14}$ s^{-1} considered "typical" of geologic processes (Fig. 6a; [2]). Under the same conditions, stresses of ~1.5 MPa are predicted in wet quartzites (Fig. 6b; [3]). At face value, Fig. 6a and b indicate that shear stresses of 50–90 MPa in the schist can be reconciled with the results of rock deformation experiments only at extreme, perhaps implausible, strain rates of $\sim 10^{-10}$ s^{-1}, and only if rheologic properties are controlled by feldspar. Given high plate convergence rates in the Late Cretaceous of ~10 cm/yr, such extreme strain rates require a shear zone ~30 m in thickness. The presence throughout the schist of asym-

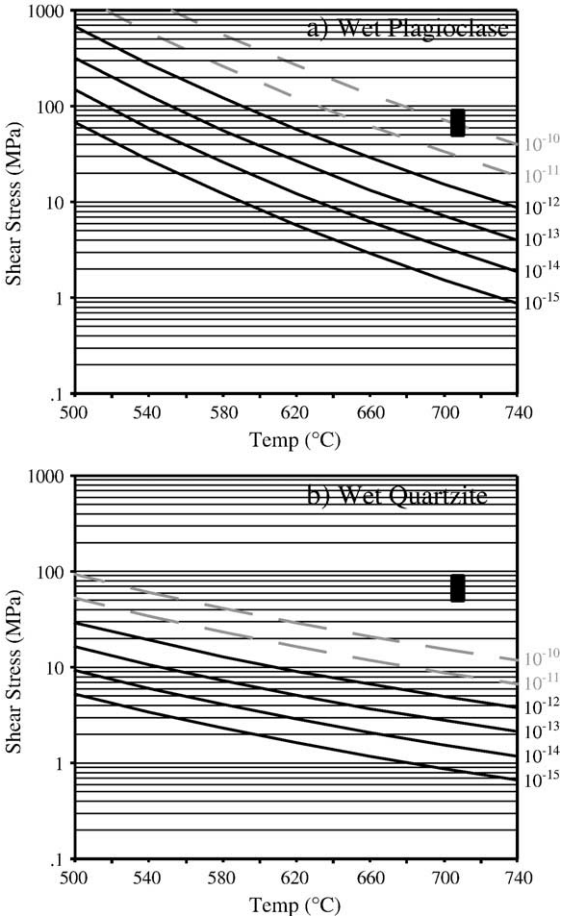

Fig. 6. Graphs representing flow laws for dislocation creep in wet plagioclase (a; [2]) and wet quartzite (b; [3]) showing rock strength at various temperatures and strain rates. Typical "geologic" strain rates [12] are indicated in black lines. Faster strain rates are shown by dashed grey lines. Conditions required by the shear heating hypothesis are shown with a black rectangle.

metric folds (e.g. Fig. 3) and widespread evidence of dislocation creep in quartz throughout the schist however suggest broadly distributed deformation. Alternatively, errors and uncertainties associated with thermobarometry and extrapolation of deformation experiment results to natural strain rates may allow for shear stresses of 50 MPa at high but "geologic" strain rates of $\sim 10^{-12}$ s^{-1} in a plagioclase-dominated deformation zone 3 km in thickness. Quartz appears to be too weak at any feasible strain rate and combination of errors to support the stresses of 50–90 MPa required by the shear heating hypothesis (Fig. 6b). The presence of biotite is additionally likely to have weakened the schist as compared to the flow laws utilized above, as Tullis and Wenk [61] found that a 15% mica-component in quartzite reduced strength by 10–50%.

The above considerations indicate that shear heating can only be considered a viable heat source for the schist at high strain rates and with rheologic properties controlled by the feldspar component. Do structural and microstructural observations support this requirement? Deformation mechanism maps of plagioclase [2] indicate that at the required temperatures and strain rates, feldspar with grain size >0.1 mm deform predominantly by dislocation creep. Evidence of dislocation creep in feldspar however is confined to only a small fraction of feldspar grains in the structurally highest (i.e. hottest) schist which shows a minor amount of undulose extinction. Evidence for extensive dislocation creep such as development of finer recrystallized grains, flattened grains containing subgrains, or development of a noticeable crystallographic preferred orientation [62] is entirely lacking. These observations suggest that deformation was dominated by diffusion creep in feldspar or largely partitioned into the weaker phases in the rock—either possibility indicates lower stresses than those associated with dislocation creep in feldspar [2]. We favor the second possibility, since in addition to the likelihood of deformation partitioning into biotite, evidence of extensive dislocation creep in quartz is ubiquitous in all thin sections of the schist. We additionally observed dynamically recrystallized, continuous and discontinuous quartz bands in roughly half of the thin sections. In deformation experiments, rock strength has been observed to approach that of quartzite as such bands develop in deforming plagioclase–quartz aggregates [60].

Another factor which may have decreased the strength of the schist as compared to experimentally deformed feldspar aggregates is evidence in the form of quartzofeldspathic veins that partial melt was present during deformation. Experimental studies show that the presence of melt can substantially reduce rock strength (e.g. [63,64]). The absence of muscovite in upper portions of the schist may also indicate melting, or a devolatilization reaction, which can also weaken rocks (e.g. [65]). Inferred presence of partial melt at temperatures of 700–800 °C has been used to justify decreasing viscosity by a factor of 5–50 compared to quartzite flow laws in thermal–mechanical models of the crust [10].

In summary, high stresses needed for extensive shear heating require that: (1) either feldspar is somewhat stronger or quartz is an order of magnitude stronger than predicted by rock deformation experiments, and despite microstructural or experimental evidence to the contrary: (2) deformation was mainly partitioned into feldspar, (3) deformation in feldspar occurred predominantly by dislocation creep, (4) a mica content of about 15% did not significantly weaken the schist, and (5) partial melting and dehydration reactions did not significantly weaken the schist. We conclude that shear heating is an unlikely heat source for the schist. Given similar high temperatures [46], tectonic history [33], and more mica and less plagioclase [66], this analysis also applies to the Pelona schist.

A final consideration related to the shear heating hypothesis and above calculations is that independent evidence indicates that middle and lower crustal rocks are significantly weaker than predicted by flow laws for dislocation creep in feldspar aggregates and quartzites. Gleason and Tullis [3] compare their quartzite flow law to geophysical models of lower crustal flow in the Basin and Range [7,8] and conclude that their flow law is "either seriously in error or the natural deformation occurred by a mechanism with a lower flow stress than that of climb-associated dislocation creep in quartz." Similarly, Ryback and Dresen [2] conclude that their flow law for dislocation creep of wet, coarse-grained feldspar requires stresses far higher than those calculated based on crustal viscosity estimates of surface displacements after major seismic events. These comparisons suggest that more efficient deformation mechanisms than dislocation creep in quartz and feldspar are widely active in the lithosphere. If such mechanisms were active in the schist, shear heating could not have significantly affected temperatures.

5.4. Alternatives to shear heating

What plausible alternatives exist for heating the schist to ~300 °C above expected temperatures? Two possible heat sources that can be quickly ruled out are advection by magmas and fluids. The absence of Salinian plutonic rocks younger than the schist argues

against advection by magmas. Significant heat advection by fluids is unlikely here and in other forearcs based on the work of Peacock [67], who modeled a scenario in which hot fluids released by metasedimentary rocks and hydrated oceanic basalt in the downgoing slab are channeled along a subduction megathrust. Peacock found that the amount of fluid available is an order of magnitude less than required to match temperatures seen in the POR schists.

One notable feature of the Southern Californian forearc in the Late Cretaceous is that the upper plate was hot (700–800 °C) as shallow subduction and schist underplating began. Thermal models by Peacock [19] and Kincaid and Sacks [22] demonstrate that hot upper plate initial conditions translate to higher subduction interface temperatures during subduction initiation than at later stages of subduction. Peacock [19], for example, found that after subducting to a depth of 30 km, the leading edge of a 45° dipping plate reaches 60% of upper plate initial temperatures. At shallower subduction dips, however, the lower plate is carried much longer distances before arriving at equivalent depths. In the case of the Sierra de Salinas, the schist was carried ~150 km beneath the western side of the Salinian arc before accreting beneath eastern-affinity batholithic rocks (Fig. 7). A longer exposure time to a hot upper plate will inevitably lead to higher temperatures in the lower plate, and we hypothesize that sufficient heat was absorbed by the schist during the initiation of shallow subduction to raise temperatures to the observed 80–95% of upper plate temperatures.

Thermal conditions at the tip of an initiating flat slab can be approximated in a 1D model in which upper plate temperatures are held constant. We constructed such a model following Philpotts [68] and find that the upper km of the schist need only be exposed to an upper plate at 800 °C for ~300,000 yr in order to reach temperatures similar to those observed in the schist. At a thrusting rate of 10 cm/yr, this would be accomplished after 30 km of thrusting. The width of the "tip," however, is an important quantity requiring the construction of a 2D thermal or thermal–mechanical model of shallow subduction initiation. Since thermal models of flat subduction have not previously been utilized in interpreting metamorphism of the POR schists [13,15,16,19], such a model would provide important constraints on the creation of inverted metamorphic gradients and a valuable test of this first order calculation.

A second, more complex conductive heating scenario is implied by Saleeby et al. [55], who present evidence that the upper plate above the Rand schist was substantially exhumed prior to metamorphism of the schist at ~9 kbar depths. This raises the possibility that the Rand Schist was conductively heated at depth prior to return flow carrying it back up to its current position relative to the upper plate. While discrimination between various scenarios for conductively heating the

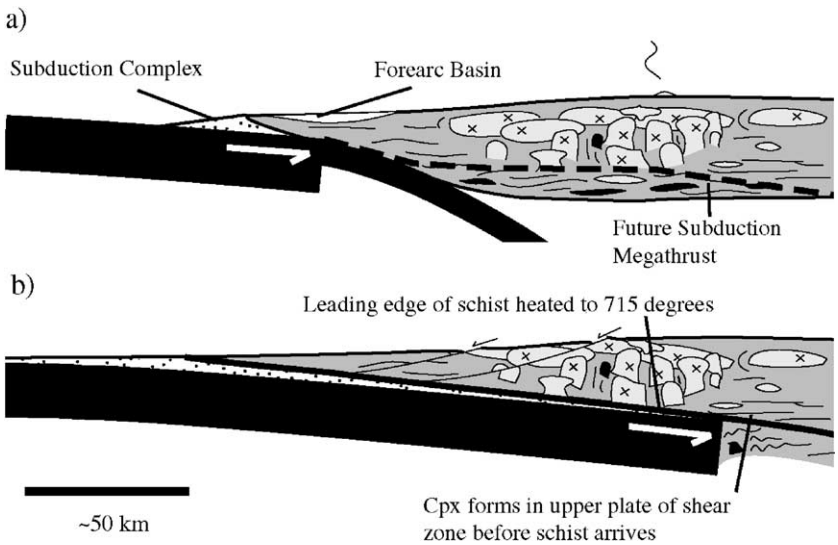

Fig. 7. Cartoons depicting Late Cretaceous subduction flattening beneath Salinia and a mechanism for conductively heating upper layers of the schist to temperatures near those of the upper plate. No vertical exaggeration. (a) Salinian continental arc just prior to collision with oncoming overthickened oceanic crust (e.g. [34]). The dashed line in panel a depicts the future location of the megathrust. (b) As lower portions of the arc were sheared off, the leading edge of the schist was carried beneath the now-extinct volcanic arc heating it to over 700°. This early-subducted schist was accreted to the upper plate.

schist is beyond the scope of this study, we conclude that conduction (of some sort) is a reasonable mechanism for heating the schist given available geologic constraints and thermal models.

5.5. Tectonic significance and analogues

The regional geology of southern California and Salinia is critically important to understanding the general evolution of subduction zones because it exposes rare crustal sections through a continental margin which underwent shallow subduction and tectonic underplating. Significant unroofing of many of the POR schists occurred along brittle or retrograde extensional faults during or immediately following underthrusting in the Late Cretaceous and Early Cenozoic as well as in the Middle Cenozoic [25,69]. In contrast, similar upper and lower plate $^{40}Ar/^{39}Ar$ muscovite and biotite cooling ages [39], a scarcity of retrograde chlorite in upper portions of the schist as compared to other schist bodies (e.g. [25]), and evidence of prograde reactions associated with ductile deformation indicate that, in the Sierra de Salinas, currently exposed upper and lower plates have undergone little separation since they were juxtaposed in the Late Cretaceous by thrusting or an early stage of extension while at high temperatures. The Sierra de Salinas thus exposes a rare window through the plutonic upper plate of the Late Cretaceous forearc into a >2 km thick succession of underplated sedimentary units.

Two key differences distinguish the Late Cretaceous forearc described here from modern forearcs. First, a temperature of at least 714 °C in the schist of Sierra de Salinas contrasts with various geologic and geophysical evidence indicating low temperatures in modern forearcs. Low heat flow (25–40 mW/m^2) typifies forearcs (e.g. [20,21,24]), a phenomenon particularly pronounced in areas of flat or shallow subduction (e.g. [70,71]). Temperature estimates in a number of kinematic and dynamic models compiled by Peacock [5] predict temperatures of 100–300 °C at depths of 40 km along subduction megathrusts, a result consistent with peak temperatures of only 300–400 °C in sediments exhumed from depths of 30 km and greater in accretionary prisms (e.g. [15,72]).

A second difference between modern subduction zones and southern California in the Late Cretaceous is the association of major upper plate extensional collapse with flat subduction and accretion of the POR schists (e.g. [25,34,38]). While detachment faulting has occurred during the past 5 Myr in the Peruvian Andes above the recently-flattened Nazca slab [73], to our knowledge there are no reported cases besides the Southern California example of large-scale collapse of an "Andean-style" margin to below sea level. A high-elevation mountain belt likely provided the potential energy for a collapse triggered by collision with overly thickened oceanic crust and associated flat subduction (e.g. [34]). Given convergence rates of ~10 cm/yr [58] and time transgressive schist underplating to the south over a period >25 m.y. [33], the flattened slab was likely buoyed by a SW trending ridge [74] on the order of 2500 km in length. The replacement of a strong, mafic arc root with a weak schist profoundly affected crustal strength [38], decoupling the upper plate from the flattened subducting slab. The appearance and heating of the schist along the base of the Salinian arc thus facilitated arc collapse.

As similar arc-collapse flat-subduction sediment-accretion events have undoubtedly occurred during at least 2.5 billion years of modern-style plate tectonics on Earth, the clues to these events are either extremely rare or with few exceptions (e.g. [75]) have gone unrecognized. Our observations demonstrate that while low temperature/pressure metamorphism typifies many former subduction complexes, subducted sediments may reach temperatures much higher than expected. Analogous events are suggested by the presence of unintruded amphibolite facies metasedimentary rocks structurally underlying arc plutonic terrains, and may be identified by thermal-chronologic relationships (e.g. [33,75]). The documentation of such events elsewhere in the geologic record would establish an important tectonic mechanism of crustal reorganization through tectonic underplating at arcs and—given the loss or "delamination" of the mafic arc root as the schist was emplaced—crustal evolution towards a more felsic composition.

6. Conclusions

We focus on quantifying and establishing the significance of high temperatures in the schist of Sierra de Salinas. It is highly unlikely that significant shear heating occurred in the schist. Evidence of partial melt, ductile deformation of quartz, and other observations indicate that the schist was incapable of supporting the necessary stresses of 50–90 MPa. Our analysis can be extended to the Pelona schist, a body previously considered a type example of shear heating.

The temperatures we observe in the schist are higher than generally seen in forearc sedimentary rocks or predicted in models of subduction zones at depths of ~40 km. Unusual circumstances were required to raise temperatures to those observed. We

propose that the schist was heated during the initiation of flat subduction at shallow levels beneath a recently active arc. The identification of analogous events in the geologic record would establish a significant mechanism of crustal reorganization and evolution toward more felsic compositions.

Acknowledgements

The manuscript benefited from extended interactions with M. Carlos, A. Martin, E. Nadin, J. Saleeby, A. Walser and P. Wetmore, as well as brief but enlightening exchanges with M. Brandon, B. Dickinson, R. Jamieson, S. Paterson, L. Rosenberg and C. Teyssier—though they may not agree with all the interpretations expressed here. Field and laboratory work was possible only by the generosity of K. Domanik, the Dorrances, Violinis, P. Kephart at the Rana Creek Ranch and M. Stromberg at the University of California Hastings Reserve. Thoughtful reviews by J. Platt and S. Peacock were appreciated. Supported by NSF EAR 0229470 (Ducea).

References

[1] A. Chrysochoos, O. Maisonneuve, G. Martin, H. Caumon, J.C. Chezeaux, Plastic and dissipated work and stored energy, Nucl. Eng. Des. 114 (1989) 323–333.
[2] E. Rybacki, G. Dresen, Deformation mechanism maps for feldspar rocks, Tectonophysics 382 (2004) 173–187.
[3] G.C. Gleason, J. Tullis, A flow law for dislocation creep of quartz aggregates determined with the molten salt cell, Tectonophysics 247 (1995) 1–23.
[4] B.W. Tichelaar, L.J. Ruff, Depth of seismic coupling along subduction zones, J. Geophys. Res. 98 (1993) 2017–2037.
[5] S.M. Peacock, Thermal structure and metamorphic evolution of subducting slabs, in: J. Eiler (Ed.), Inside the Subduction Factory, Geophys. Monogr., vol. 138, 2003, pp. 7–22.
[6] R.J. Stern, Subduction zones, Rev. Geophys. 40 (2002), doi:10.1029/2001RG000108.
[7] L. Block, L.H. Royden, Core complex geometries and regional scale flow in the lower crust, Tectonics 9 (1990) 557–567.
[8] S. Kruse, M. McNutt, J. Phipps-Morgan, L. Royden, B. Wernicke, Lithospheric extension near Lake Mead, Nevada: a model for ductile flow in the lower crust, J. Geophys. Res. 96 (1991) 4435–4456.
[9] B. Wernicke, S. Getty, Intracrustal subduction and gravity currents in the deep crust: Sm–Nd, Ar–Ar, and thermobarometric constraints from the Skagit Gneiss Complex, Washington, GSA Bull. 109 (1997) 1149–1166.
[10] R.A. Jamieson, C. Beaumont, S. Medvedev, M.H. Nguyen, Crustal channel flows: 2. Numerical models with implications for metamorphism in the Himalayan–Tibetan orogen, J. Geophys. Res. 109 (2004), doi:10.1029/2003JB002811.
[11] M. Clark, L.H. Royden, Topographic ooze: building the eastern margin of Tibet by lower crustal flow, Geology 28 (2000) 703–706.
[12] B.A. van der Pluijm, S. Marshak, Earth Structure: An Introduction to Structural Geology and Tectonics, McGraw Hill, 1997.
[13] C.M. Graham, P.C. England, Thermal regimes and regional metamorphism in the vicinity of overthrust faults: an example of shear heating and inverted metamorphic zonation from southern California, Earth Planet. Sci. Lett. 31 (1976) 142–152.
[14] C.H. Scholz, Shear heating and the state of stress on faults, J. Geophys. Res. 85 (1980) 6174–6184.
[15] S.M. Peacock, Blueschist-facies metamorphism, shear heating, and P-T-t paths in subduction shear zones, J. Geophys. Res. 97 (1992) 17693–17707.
[16] P.C. England, P. Molnar, The interpretation of inverted metamorphic isograds using simple physical calculations, Tectonics 12 (1993) 145–157.
[17] T.M. Harrison, M. Grove, O.M. Lovera, E.J. Catlos, A model for the origin of Himalayan anatexis and inverted metamorphism, J. Geophys. Res. 103 (1998) 27017–27032.
[18] A. Camacho, I. McDougall, R. Armstrong, J. Braun, Evidence for shear heating, Musgrave Block, central Australia, J. Struct. Geol. 23 (2001) 1007–1013.
[19] S.M. Peacock, Creation and preservation of subduction-related inverted metamorphic gradients, J. Geophys. Res. 92 (1987) 12763–12781.
[20] Y. Furukawa, S. Uyeda, Thermal state under the Tohoko Arc with consideration of crustal heat generation, Tectonophysics 164 (1989) 175–187.
[21] R.D. Hyndman, K. Wang, The rupture zone of Cascadia great earthquakes from current deformation and the thermal regime, J. Geophys. Res. 100 (1995) 22133–22154.
[22] C. Kincaid, I.S. Sacks, Thermal and dynamical evolution of the upper mantle in subduction zones, J. Geophys. Res. 102 (1997) 12295–12315.
[23] A.D. Huerta, L.H. Royden, K.V. Hodges, The thermal structure of collisional orogens as a response to accretion, erosion, and radiogenic heating, J. Geophys. Res. 103 (1998) 15287–15302.
[24] R. Von Herzen, C. Ruppel, P. Molnar, M. Nettles, S. Nagihara, G. Ekstrom, A constraint on the shear stress at the Pacific–Australian plate boundary from heat flow and seismicity at the Kermadec forearc, J. Geophys. Res. 106 (2001) 6817–6833.
[25] C.E. Jacobson, M. Grove, A. Vucic, J.N. Pedrick, Exhumation of the Orocopia Schist and associated rocks of southeastern California: relative roles of erosion, synsubduction tectonic denudation, and middle Cenozoic extension, in: M. Cloos, W.D. Carlson, M.C. Gilbert, J.G. Liou, S.S. Sorensen (Eds.), Convergent Margin Terranes and Associated Regions—A Tribute to W.G. Ernst, Geologic Society of America Special Paper, in press.
[26] J.H. Davies, D.J. Stevenson, Physical model of source region of subduction zone volcanics, J. Geophys. Res. 97 (1992) 2037–2070.
[27] Y. Furukawa, Depth of the decoupling plate interface and thermal structure under arcs, J. Geophys. Res. 98 (1993) 20005–20013.
[28] D.C. Ross, Metagraywacke in the Salinian block, central coast ranges, California—and a possible correlative across the San Andreas fault, J. Res. U.S. Geol. Surv. 4 (1976) 683–696.
[29] J.M. Mattinson, Petrogenesis and evolution of the Salinian magmatic arc, in: J.L. Anderson (Ed.), The Nature and Origin of Cordilleran Magmatism, Memoir-Geological Society of America, vol. 174, Geological Society of America (GSA), Boulder, CO, United States, 1990, pp. 237–250.

[30] R.C. Schott, C.M. Johnson, Sedimentary record of the Late Cretaceous thrusting and collapse of the Salinia–Mojave magmatic arc, Geology (Boulder) 26 (1998) 327–330.
[31] D.L. Barbeau, M.N. Ducea, G.E. Gehrels, S.B. Kidder, P.H. Wetmore, J.B. Saleeby, U–Pb detrital–zircon geochronology of northern Salinian basement and cover rocks, Geol. Soc. Amer. Bull. 117 (2005), doi:10.1130/B25496.25491.
[32] R.E. Powell, Balanced palinspastic reconstruction of pre-late Cenozoic paleogeology, Southern California: geologic and kinematic constraints on evolution of the San Andreas fault system, in: R.E. Powell, R.J. Weldon II, J.C. Matti (Eds.), The San Andreas Fault System; Displacement, Palinspastic Reconstruction, and Geologic Evolution, Memoir-Geological Society of America, vol. 178, Geological Society of America (GSA), Boulder, CO, United States, 1993, pp. 1–106.
[33] M. Grove, C.E. Jacobson, A.P. Barth, A. Vucic, Temporal and spatial trends of Late Cretaceous–early Tertiary underplating of Pelona and related schist beneath southern California and southwestern Arizona, Geol. Soc. Amer., Spec. Pap. 374 (2003).
[34] J.B. Saleeby, Segmentation of the Laramide Slab-evidence from the southern Sierra Nevada region, GSA Bull. 115 (2003) 655–668.
[35] S.B. Kidder, M.N. Ducea, G. Gehrels, P.J. Patchett, J. Vervoort, Tectonic and magmatic development of the Salinian Coast Ridge Belt, California, Tectonics 22 (2003), doi:10.1029/2002TC001409.
[36] R.W. Kistler, D.E. Champion, Rb–Sr whole-rock and mineral ages, K–Ar, (super 40) Ar/(super 39) Ar, and U–Pb mineral ages, and strontium, lead, neodymium, and oxygen isotopic compositions for granitic rocks from the Salinian Composite Terrane, California, U. S. Geological Survey, Reston, VA, 2001, 83 pp.
[37] W.R. Dickinson, M.N. Ducea, L.I. Rosenberg, H.G. Greene, S.A. Graham, J.C. Clark, G.E. Weber, S.B. Kidder, W.G. Ernst, E.E. Brabb, Net Dextral Slip, Neogene San Gregorio-Hosgri Fault Zone, Coastal California: Geologic Evidence and Tectonic Implications, Geologic Society of America, Boulder, 2005, 43 pp.
[38] P.E. Malin, E.D. Goodman, T.L. Henyey, Y.G. Li, D.A. Okaya, J.B. Saleeby, Significance of seismic reflections beneath a tilted exposure of deep continental crust, Tehachapi Mountains, California, J. Geophys. Res. 100 (1995) 2069–2087.
[39] A.P. Barth, J.L. Wooden, M. Grove, C.E. Jacobson, J.N. Pedrick, U–Pb zircon geochronology of rocks in the Salinas Valley region of California: a reevaluation of the crustal structure and origin of the Salinian block, Geology 31 (2003) 517–520.
[40] R.C. Schott, C.M. Johnson, Garnet-bearing trondhjemite and other conglomerate clasts from the Gualala basin, California: sedimentary record of the missing western portion of the Salinian magmatic arc? Geol. Soc. Amer. Bull. 113 (2001) 870–880.
[41] J.J. Papike, Chemistry of the rock-forming silicates: multiple-chain, sheet, and framework structures, Rev. Geophys. 26 (1988) 407–444.
[42] J.M. Ferry, F. Spear, Experimental calibration of the partitioning of Fe and Mg between biotite and garnet, Contrib. Mineral. Petrol. 66 (1978) 113–117.
[43] J. Ganguly, W. Cheng, M. Tirone, Thermodynamics of aluminosilicate garnet solid solution; new experimental data, an optimized model, and thermometry applications, Contrib. Mineral. Petrol. 126 (1996) 137–151.
[44] M.J. Holdaway, B. Mujhopadhyay, M.D. Dyar, C.V. Guidotti, B.L. Dutrow, Garnet–biotite geothermometry revised: new Margules parameters and a natural specimen data set from Maine, Am. Mineral. 82 (1997) 582–595.
[45] C. Zhu, D.A. Sverjensky, F–Cl–OH partitioning between biotite and apatite, Geochim. Cosmochim. Acta 56 (1992) 3435–3467.
[46] C.M. Graham, R. Powell, A garnet–hornblende geothermometer: calibration, testing, and application to the Pelona Schist, Southern California, J. Metamorph. Geol. 2 (1984) 13–31.
[47] T.D. Hoisch, Equilibria within the mineral assemblage quartz+muscovite+biotite+garnet+plagioclase, and implications for the mixing properties of octahedrally-coordinated cations in muscovite and biotite, Contrib. Mineral. Petrol. 108 (1991) 43–54.
[48] J.H. Kruhl, Prism- and basal-plane parallel subgrain boundaries in quartz: a microstructural geothermobarometer, J. Metamorph. Geol. 14 (1996) 581–589.
[49] F. Spear, An experimental study of hornblende stability and compositional variability in amphibole, Am. J. Sci. 281 (1981) 697–734.
[50] F.S. Spear, Metamorphic Phase Equilibria and Pressure–Temperature–Time Paths, Washington, DC, 1993, 799 pp.
[51] M.J. Kohn, F. Spear, Retrograde net transfer reaction insurance for pressure–temperature estimates, Geology 28 (2000) 1127–1130.
[52] R.T. Cygan, A.C. Lasaga, Self-diffusion of magnesium in garnet at 750° to 950°, Am. J. Sci. 285 (1985) 328–350.
[53] B.R. Hacker, J.L. Mosenfelder, Metamorphism and deformation along the emplacement thrust of the Samail ophiolite, Oman, Earth Planet. Sci. Lett. 144 (1996) 435–451.
[54] C. Jacobson, The (super 40) Ar/ (super 39) Ar geochronology of the Pelona Schist and related rocks, Southern California, J. Geophys. Res. 95 (1990) 509–528.
[55] J.B. Saleeby, K.A. Farley, R.W. Kistler, R. Fleck, Thermal evolution and exhumation of deep level batholithic exposures, southernmost Sierra Nevada, California, in: M. Cloos, W.D. Carlson, M.C. Gilbert, J.G. Liou, S.S. Sorensen (Eds), Convergent margin terranes and associated regions—a tribute to W.G. Ernst, Geologic Society of America Special Paper, in press.
[56] I. McDougall, T.M. Harrison, Geochronology and Thermochronology by the (super 40) Ar/ (super 39) Ar Method, Second edition, Oxford University Press, New York, 1999, 269 pp.
[57] R.A. Jamieson, C. Beaumont, J. Hamilton, P. Fullsack, Tectonic assembly of inverted metamorphic sequences, Geology 24 (1996) 839–842.
[58] J. Stock, P. Molnar, Uncertainties and implications of the Late Cretaceous and Tertiary position of North America relative to the Farallon, Kula, and Pacific plates, Tectonics 7 (1988) 1339–1384.
[59] M. Bjørnerud, H. Austrheim, Comment on: "Evidence for shear heating, Musgrave Block, central Australia" by A. Camacho, I. McDonald, R. Armstrong, and J. Braun, J. Struct. Geol. 24 (2002) 1537–1538.
[60] L.N. Dell'Angelo, J. Tullis, Textural and mechanical evolution with progressive strain in experimentally deformed aplite, Tectonophysics 256 (1996) 57–82.
[61] J. Tullis, H.R. Wenk, Effect of muscovite on the strength and lattice preferred orientations of experimentally deformed quartz aggregates, Mater. Sci. Eng., A Struct. Mater.: Prop. Microstruct. Process. 175 (1994) 209–220.
[62] J. Tullis, Experimental studies of deformation mechanisms and microstructures in quartzo–feldspathic rocks, in: D.J. Barber,

P.G. Meredith (Eds.), Deformation Processes in Minerals, Ceramics and Rocks, Unwin Hyman, London, 1990, pp. 190–227.
[63] T. Rushmer, Volume change during partial melting reactions: implications for melt extraction, melt geochemistry and crustal rheology, Tectonophysics 342 (2001).
[64] J. Mecklenburgh, E.H. Rutter, On the rheology of partially molten synthetic granite, J. Struct. Geol. 25 (2003) 1575–1585.
[65] E.H. Rutter, K.H. Brodie, Mechanistic interactions between deformation and metamorphism, Geol. J. 30 (1995) 227–240.
[66] C.E. Jacobson, Relationship of deformation and metamorphism of the Pelona schist to movement on the Vincent thrust, San Gabriel Mountains, Southern California, Am. J. Sci. 283 (1983) 587–604.
[67] S.M. Peacock, Thermal effects of metamorphic fluids in subduction zones, Geology 15 (1987) 1057–1060.
[68] A.R. Philpotts, Principles of Igneous and Metamorphic Petrology, Prentice-Hall College Div., 1990, 494 pp.
[69] A. Yin, Passive-roof thrust model for the emplacement of the Pelona–Orocopia Schist in southern California, United States, Geology (Boulder) 30 (2002) 183–186.
[70] J.P. Ziagos, D.D. Blackwell, F. Mooser, Heat flow in southern Mexico and the thermal effects of subduction, J. Geophys. Res. 90 (1985) 5410–5419.
[71] S.G. Henry, H.N. Pollack, Terrestrial heat flow above the Andean subduction zone in Bolivia and Peru, J. Geophys. Res. 93 (1988) 15153–15162.
[72] S. Schwarz, B. Stockhert, Pressure solution in siliciclastic HP-LT metamorphic rocks—constraints on the state of stress in deep levels of accretionary complexes, Tectonophysics 255 (1995) 203–209.
[73] B. McNulty, D. Farber, Active detachment faulting above the Peruvian flat slab, Geology (Boulder) 30 (2002) 567–570.
[74] A. Barth, J. Schneiderman, A comparison of structures in the Andean Orogen of Northern Chile and exhumed midcrustal structures in Southern California, USA: an analogy in tectonic style? Int. Geol. Rev. 38 (1996) 1075–1085.
[75] J.E.P. Matzel, S.A. Bowring, R.B. Miller, Protolith age of the Swakane Gneiss, North Cascades, Washington: evidence of rapid underthrusting of sediments beneath an arc, Tectonics 23 (2004).
[76] T.W. Dibblee, Jr., Geologic map of the Soledad quadrangle and Jamesburg quadrangle, California, U.S. Geological Survey Open-File Map 74-1021, 1972.